A Self-Powered Supply-Sensing Biosensor Platform Using Bio Fuel Cell and Low-Voltage, Low-Cost CMOS Supply-Controlled Ring Oscillator With Inductive-Coupling Transmitter for Healthcare IoT

Kiichi Niitsu, *Member, IEEE*, Atsuki Kobayashi, *Student Member, IEEE*, Yuya Nishio, *Student Member, IEEE*, Kenya Hayashi, *Student Member, IEEE*, Kei Ikeda, *Student Member, IEEE*, Takashi Ando, Yudai Ogawa, Hiroyuki Kai, Matsuhiko Nishizawa, and Kazuo Nakazato

***Abstract*— This paper proposes a self-powered disposable supply-sensing biosensor platform for big-data-based healthcare applications. The proposed supply-sensing biosensor platform is based on bio fuel cells and a 0.23-V 0.25-μm zero-V_{th} all-digital CMOS supply-controlled ring oscillator with a current-driven pulse-interval-modulated inductive-coupling transmitter. The fully digital, and current-driven architecture uses zero-V_{th} transistors, which enables low voltage operation and a small footprint, even in a cost-competitive legacy CMOS. This enables converterless self-powered operation using a bio fuel cell, which is ideal for disposable healthcare applications. To verify the effectiveness of the proposed platform, a test chip was fabricated using 0.25-μm CMOS technology. The experimental results successfully demonstrate operation with a 0.23-V supply, which is the lowest supply voltage reported for proximity transmitters. A self-powered biosensing operation using organic bio fuel cells was also successfully demonstrated. In addition, an asynchronous inductive-coupling receiver and an off-chip inductor for performance improvement were successfully demonstrated.**

***Index Terms*— Sugar monitoring, CMOS, healthcare, point-of-care testing, wearable computing.**

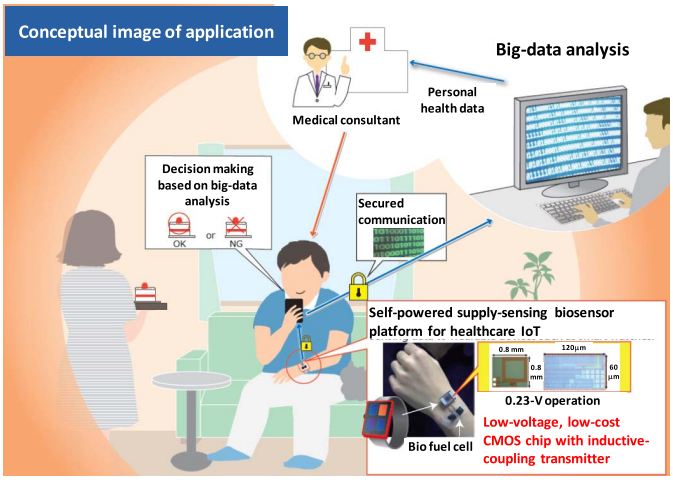

Fig. 1. Conceptual diagram of the application of the proposed supply-sensing biosensor platform.

I. Introduction

ENSURING stable energy is one of the most important current challenges in wearable and implantable healthcare devices associated with big-data analysis (Fig. 1). To address this issue, many developments with respect to batteries [1], wireless power delivery [2], and energy harvesting [3] have been reported. Although technical improvements in these areas have been rapid, none of them fully satisfy the requirements. Batteries are unsuitable for use near the human body for safety reason. Even though encased batteries are commonly used in pacemakers, some people do not want to accept in-body battery from psychological reason. Besides, generally speaking encased batteries are costly. Wireless power delivery requires a large power-receiving antenna, and energy harvesting is unstable for healthcare application. Additionally, the latter two approaches require power management units such as power receivers, AC-DC converters, and DC-DC converters which consume area and increase cost.

As an alternative energy source, bio fuel cells have been intensely developed for applications such as disposable transdermal iontophoresis patches [4]–[6] and brain-machine

Manuscript received December 9, 2016; revised May 19, 2017, September 24, 2017, and December 21, 2017; accepted December 29, 2017. Date of publication March 28, 2018; date of current version August 3, 2018. This work was supported in part by Precursory Research for Embryonic Science and Technology, Japan Science and Technology Agency, in part by a Grant-in-Aid for Scientific Research under Grant 20226009 and Grant 25220906, in part by Grants-in-Aid for Young Scientists (A) under Grant 16H06088 from the Ministry of Education, Culture, Sports, Science, and Technology of Japan, in part by the Strategic Information and Communications Research and Development Promotion Programme under Grant 121806006 and Grant 152106004 of the Ministry of Internal Affairs and Communications, Japan, in part by TOYOTA RIKEN, and in part by The Nitto Foundation. This paper was recommended by Associate Editor E. Sanchez-Sinencio. *(Corresponding author: Kiichi Niitsu.)*

K. Niitsu is with Nagoya University, Nagoya 464-8603, Japan, and also with Precursory Research for Embryonic Science and Technology, Japan Science and Technology Agency, Saitama 332-0012, Japan (e-mail: niitsu@nuee.nagoya-u.ac.jp).

A. Kobayashi, Y. Nishio, K. Hayashi, K. Ikeda, T. Ando, and K. Nakazato are with Nagoya University, Nagoya, Japan.

Y. Ogawa, H. Kai, and M. Nishizawa are with Tohoku University, Sendai, Japan.

Color versions of one or more of the figures in this paper are available online at http://ieeexplore.ieee.org.

Digital Object Identifier 10.1109/TCSI.2018.2791516

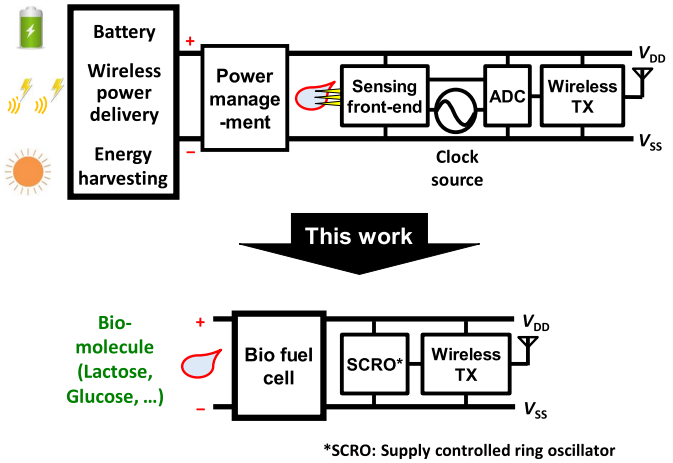

Fig. 2. Proposed supply-sensing biosensor platform compared to conventional platforms.

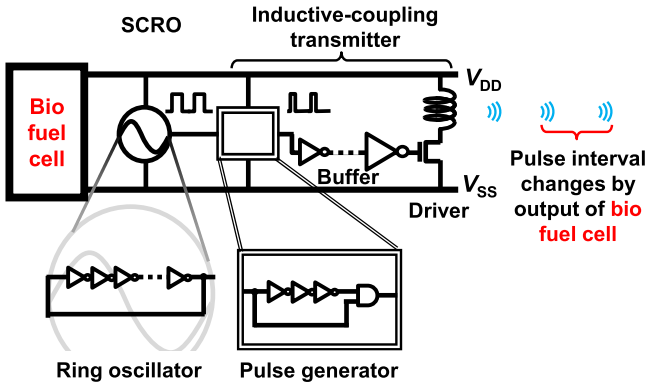

Fig. 3. Circuit diagram of the proposed supply-sensing biosensor platform.

interfaces [4]. Bio fuel cells are safe, stable and do not require an antenna or AC-DC converter. Additionally, the amount of energy obtained from the human body can be used as bio sensing data, and thus the sensor electrodes and front-ends become unnecessary. Of the bio fuel cells, the organic bio fuel cell [4]–[6] is especially promising because it is cheap and environmentally friendly, which enables disposable healthcare. However, the output supply voltage from a bio fuel cell is usually lower than 0.4 V, and conventional circuits cannot operate using bio fuel cells without power management circuits. Thus, a new circuit technique must be developed for converter-less operation.

This paper introduces a supply-sensing biosensor platform using a bio fuel cell and a 0.23-V 0.25-μm zero-V_{th} all-digital CMOS SCRO with a current-driven, pulse interval-modulated, inductive-coupling transmitter (Fig. 2). Compared with conventional architecture [7]–[18], the required area and power can be dramatically reduced. In addition to the contribution in conference publication [19], the present paper describes the proposed design principle for the supply-sensing platform, receiver design for inductive-coupling communication and its demonstration of intra-chip communication, and design using off-chip inductor.

Our objective is self-powered sensor where size and cost are limited. For example, wearable sensors and cavitas sensors are our target applications. In the existing sensors, the battery and electronics dominates their size and cost. Thus, by applying our proposed technique, their size and cost can be dramatically reduced.

This paper is organized as follows: the proposed supply-sensing biosensor platform and its design principle are introduced in Section II. The design of the prototype CMOS sensor and measurement setup are summarized in Section III. Sections IV and V present the measurement results and demonstration of the self-powered operation, respectively. Section VI presents the design and results of the receiver for demonstrating feasibility of proximity communication. Section VII introduces the design and experimental verification of the proposed platform with off-chip inductor for further cost reduction. Section VIII concludes this paper.

II. Supply-Sensing Biosensor Platform

A. Basic Principles

Fig. 3 shows the circuit diagram of the proposed supply-sensing biosensor platform, which consists of three parts: the bio fuel cells, SCRO, and an inductive-coupling transmitter. The different points from the conventional topologies are followings:

- Elimination of the power management circuits, clock sources, and ADCs.
- Introduction of digital-based SCRO.
- Introduction of current-driven inductive-coupling transmitter.

By eliminating the area-hungry power management circuits, sensing front-end circuit, power-hungry clock source such as PLLs, and power-hungry analog-to-digital converters (ADC), the occupied area and required power can be dramatically reduced. By introducing digital-based SCRO, the required minimum supply voltage can be reduced. By introducing the current-driven inductive-coupling link, low-voltage operation can be possible.

To minimize the supply voltage, a fully digital, current-driven architecture was employed. Implementing the proposed architecture using zero-V_{th} transistors enables a low-supply voltage of less than 0.4 V to be used. Zero-V_{th} transistors are commonly available on both the state-of-the-art and legacy CMOS technologies. Thus, our technique can be feasible even in other technologies. Because the supply-sensing scheme is unsuitable for pulse amplitude modulation owing to its nature, time-domain modulation must be employed. To minimize power consumption, pulse-interval modulation (PIM) was employed in this work as shown in Fig. 4.

The overall platform must be designed considering the performance of bio fuel cells. Fig. 5 illustrates the typical design considerations for the proposed supply-sensing biosensor platform using bio fuel cells. Output current and power of the bio fuel cells changes as a function of the load resistance. In general, higher output current can be obtained at lower output voltages from typical bio fuel cells. By taking into account the size of bio fuel cells and resistance of the load (in our case, the CMOS chip), we have optimized the overall design.

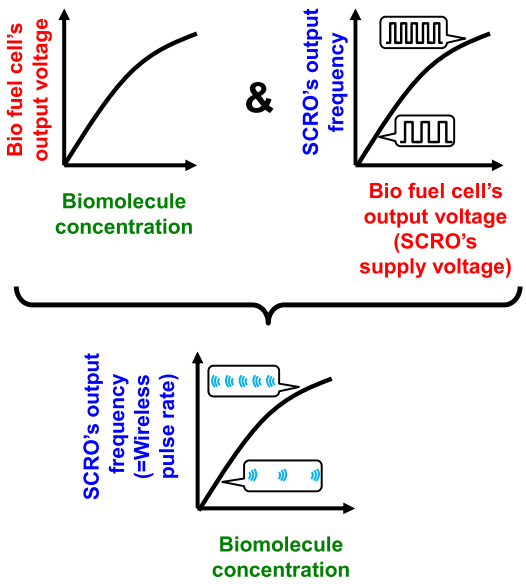

Fig. 4. Operation principles of the proposed supply-sensing biosensor platform. Pulse interval modulation (PIM) is adopted.

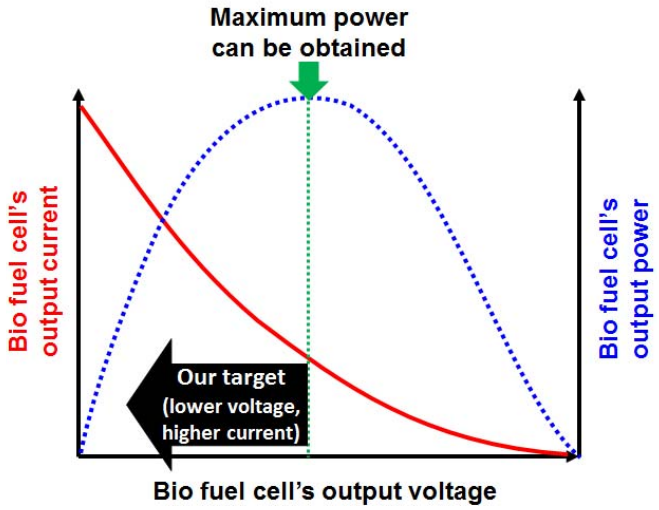

Fig. 5. Design guideline of the overall platform with consideration of bio fuel cell's output current and power.

The voltage is determined by the relationship between the impedances of the bio fuel cells and CMOS circuit load. By optimizing the internal resistance of the bio fuel cells and the load resistance of CMOS circuits, we ensure being operating at an specific low voltage in maximum power point curve. The resistance of the bio fuel cell can be designed by enzyme amount and its size. While, the resistance of the CMOS chip can be designed by changing the size of the transistors.

The oscillating function of SCRO allows us to have withered a constant current and voltage. As we have confirmed by measurement, the voltage and current constantly vary.

In the design of current-driven inductive-coupling link, the most important aspect to ensure communication performance is to obtain sufficient transmitter current. Obtaining current is more important than obtaining power. Besides, since our design utilized zero-V_{th} transistors which causes large leakage current, we adopt this design guideline. Thus, a lower supply voltage is preferred for reliable operation of a current-driven inductive-coupling transmitter. To obtain the maximum power from bio fuel cells, the platform should be designed to operate under the voltage at which it can obtain the maximum power. However, the available current is not maximized at that point. Hence, to operate the current-driven inductive-coupling transmitter, a lower supply voltage is preferred.

B. Bio Fuel Cell

In the proposed supply-sensing biosensor platform, the bio fuel cell has two functions: energy harvesting and front-end sensing. Typical bio fuel cells can generate a voltage of less than 0.4 V [4]–[6]. Thus, to realize self-powered operation without large and expensive power management circuits such as up-converters, the circuits must operate with a supply voltage of less than 0.4 V.

In order for bio fuel cells to function as both a power source and sensing front-end, the anode and cathode must be designed carefully. Unlike typical biosensors based on one transducer, the proposed supply-sensing biosensor uses two transducers (anode and cathode). Thus, if the output power depends on unintended transducers, the proposed device cannot function as a sensor even if it functions well as power source.

For aiming practical application, glucose or lactate fuel cells are beneficial because it can be used for glucose or lactate monitoring. However, they are under development and not available for us. As a preliminary study, we have chosen fructose fuel cell. Though fructose is not available on the human body and it has no healthcare application, it is meaningful as a preliminary study. Since the energy generation mechanism of fructose fuel cell is similar to that of glucose and lactate fuel cells, this study will contribute the successive research and development.

In the case of our prototype fructose sensor, we use the following reactions: in the anode, the capability to product current depends on fructose concentration. In the cathode, the capability to product current depends on oxygen concentration. To sense fructose, the total output current must depend on not oxygen but fructose, which we achieve by adjusting the sizes of the anode and cathode.

The biofuel cell in this work is an enzymatic fuel cell. Fig. 8(a) shows the conceptual image of the mechanism of power generation from the bio fuel cells. Two kinds of enzymes, d-fructose dehydrogenase (FDH; EC 1.1.99.11, 169.9 U mg^{-1}, ca. 140 kDa, from *Gluconobactor*, purchased from Toyobo Enzyme Co.) and laccase (LAC; EC 1.10.3.2, 108 U mg^{-1}, ca. 60 kDa, from *Trametes* sp, purchased from Daiwa Kasei Co.) are immobilized to anode and cathode, respectively. They can directly catalyze the oxidation of D-fructose and the reduction of dioxygen, respectively. We used the FDH as received without further purification. While, the LAC was purified by anion exchange chromatography with a DEAE-Toyoperal column.

It is really important for the bio fuel cells to be safe in human use from the viewpoint of practical application. These enzymes are safe and suitable for human use. By exploiting these enzymes, following chemical reactions are occurred.

$$\text{Anode} : O_2 + 2H^+ \rightarrow H_2O$$
$$\text{Cathode} : \text{Fructose} \rightarrow \text{5-Keto-D-Fructose} + 2H^+$$

As a result of the above chemical reaction, electrons are transferred from the anode to cathode, and energy can be available at the load devices.

Fig. 8(b) shows a detailed equivalent electrical circuit model of the bio fuel cell. The model is based on the literature [36]. The bio fuel cells can be modeled as combination of the internal resistance, R_{int}, the output source voltage, V_{src}, the ohmic resistance, R_{ohm}, and the internal capacitance, C_{int}.

Fig. 8(c) shows a simplified equivalent electrical circuit model of the bio fuel cell. Since the values of R_{ohm} and C_{int} are relatively smaller than those of R_{int} and V_{src}. The bio fuel cells can be simply modeled as series of R_{int} and V_{src}.

C. SCRO

To achieve PIM, the supply voltage must be modulated using pulse intervals. To enable low-voltage operation, we implemented an SCRO. The SCRO consists of a normal ring oscillator with inverter cells. As the inverter cell, the standard cell using one NMOS and one PMOS from the foundry were utilized.

In the SCRO design, the number of stages should be optimized for low area consumption and low power consumption. Area consumption is determined by the number of stages of SCRO. Our target is low-cost implementation, and thus area consumption should be minimized within the acceptable power budget from the biofuel cell. As well as area consumption, the number of stages of SCRO have also impacts on power consumption.

Since the power consumption of SCRO is much smaller than that of the inductive-coupling transmitter, the duty ratio (on/off ratio) is the most important factor that determines the total power consumption. Besides, since the minimum pulse width is determined by the bandwidth of the inductive-coupling channel, the output frequency of the SCRO is the most important factor which determines the duty ratio and thus the total power consumption.

In the design of SCRO, the designer also must determine the target frequency while considering the performance of the inductive-coupling receiver. For recovering transmitted frequency signal at the receiver side, the target frequency must be lower than the maximum operational frequency of the receiver. In the literature, high-speed (over 10GHz) inductive-coupling receiver design [8] has been reported. The designer can choice the receiver architecture while considering the SCRO and receiver design.

A higher number of stages increases the area consumption and decreases total power consumption. Due to our target being a low-cost implementation with acceptable power consumption, the number of stages was reduced as small as possible. In this work, seventeen stages were used for the prototype with an on-chip inductor. For the prototype with an off-chip inductor, 101 stages were used because the demand for area reduction was relatively relaxed.

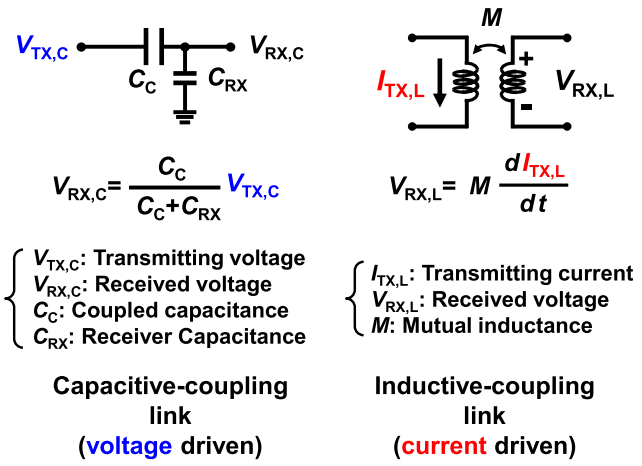

Fig. 6. Operating principle of two kinds of the proximity communication techniques.

D. Low Supply Voltage Inductive-Coupling Transmitter

For the wireless transmitter, we implemented a current-driven, inductive-coupling transmitter. Considering the limited power budget, proximity communication without any security protection was adopted. Commonly-used electrical proximity communication can be categorized into two approaches: the capacitive-coupling links and inductive-coupling links. Fig. 6 shows their conceptual operating principles. The voltage obtained at the receiver side of a capacitive-coupling link is determined by the ratio of the coupled capacitance to the total capacitance. Thus, a voltage that is higher than the transmit voltage cannot be received.

In contrast, the voltage received in the inductive-coupling link is determined by a product of the slew rate of the transmit current and mutual inductance. A high received voltage can be obtained, even with a low supply-voltage transmitter. Bio fuel cells can generate larger currents at lower voltages because of their characteristics [4]; thus, a current-driven inductive-coupling link is preferable.

To minimize power supply voltage while reaping the advantages of inductive-coupling, the proposed inductive-coupling transmitter was designed to be as simple as possible. As shown in Fig. 3, it consists of a pulse generator, buffers, driver, and inductor. The pulse generator consists of an inverter chain and an AND gate, which converts the clock signal into a low-duty pulse signal.

Fig. 7 compares the performance of the proposed method with other state-of-the-art proximity communications. There is a trade-off between power supply voltage and the technology node. The lowest supply voltage was 0.7 V [35] for the clock-based synchronous inductive-coupling link, and none of the conventional proximity communications could satisfy the requirement for operation with bio fuel cells. This work achieved the lowest supply voltage using the most cost-competitive technology node.

The inductive-coupling transmitter was designed as described in [21]. The diameter of the inductor is determined

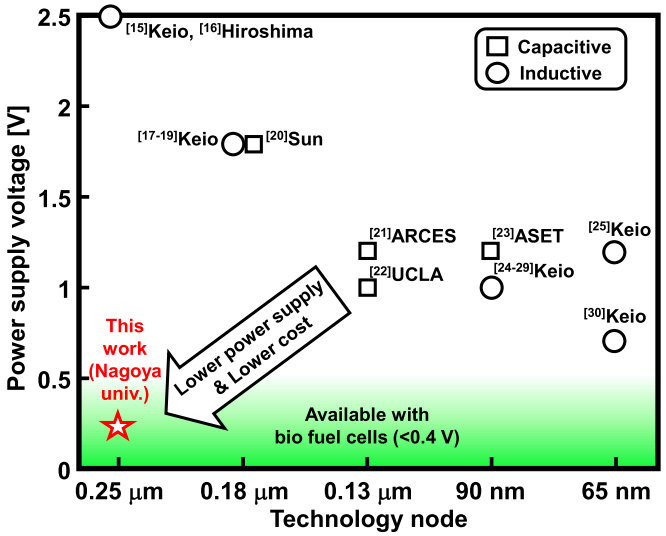

Fig. 7. Performance comparison with the state-of-the-art proximity communications.

by the communication distance. Because of the considerable degradation of magnetic flux strength as a function of communication distance, the communication distance only can be extended to be almost same as the inductor's diameter. The inductive-coupling transmitter consists of the pulse generator, the driver, and the inductor.

The pulse generator reduces power consumption by reducing the on-time of the driver (duty cycle of the transmit pulse). In the pulse generator, the number of inverter chain stages determines the pulse width. This number should be odd for pulse generation. In this work, we use five stages by considering the bandwidth of the inductive-coupling channel characteristic.

The transmit current and driver size must be designed considering the communication channel and receiver circuit. The proposed platform uses asynchronous architecture. Thus, an asynchronous receiver must be adopted. In [17], the required level of voltage to drive the asynchronous receiver is more than 100 mV. The transmitter should be designed to transmit sufficient current for reliable operation.

The inductor can be implemented in two ways as an on-chip inductor on CMOS circuits, or an off-chip inductor on a PCB board. For low-cost chip implementation, an off-chip inductor is preferable. In this study, we used both an on-chip and off-chip inductors. The equivalent circuit model of the inductor shown in Fig. 9 was utilized for simulation. The parameters of the equivalent circuit model were calculated using [15].

E. Testing Method for Reliable Operation

This subsection discusses the testing method of the supply-sensing platform for reliable operation. For practical application, it is essential to ensure that the output power of bio fuel cell does not collapse after connecting the CMOS chip including the SCRO and wireless transmitter. In order to guarantee the reliable operation, we have proposed a testing method.

The test procedure is as followings:

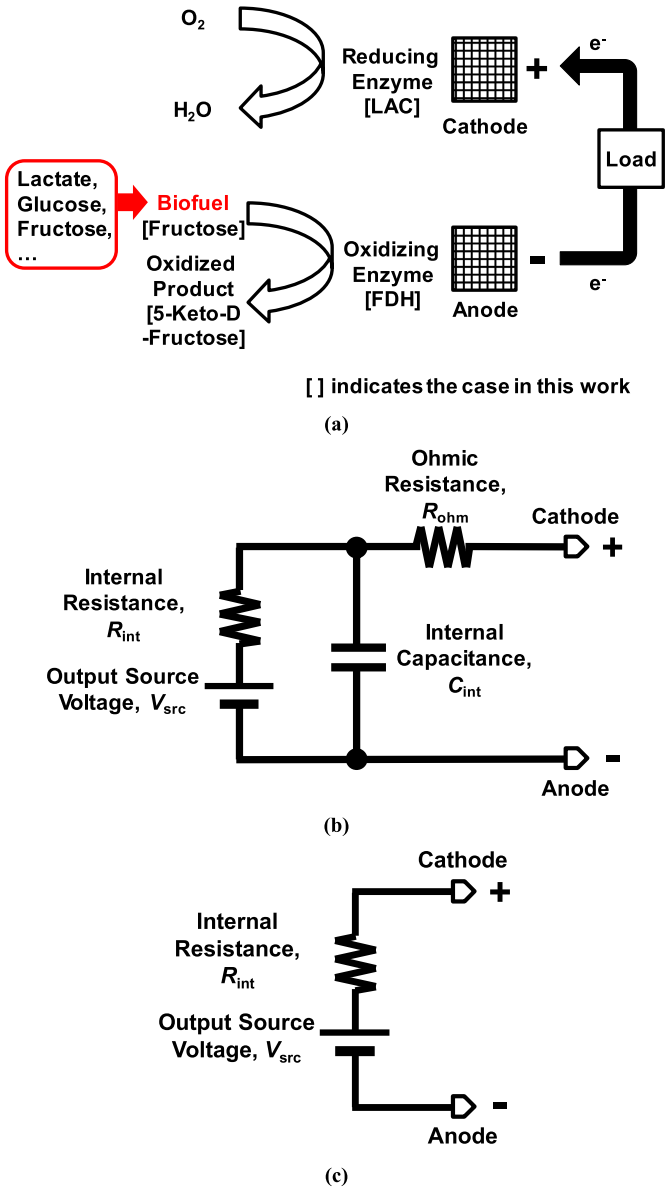

Fig. 8. Conceptual image of the mechanism of power generation from the bio fuel cells (a), its detailed equivalent electrical circuit model (b), and its simplified equivalent electrical circuit model (c).

Test1: Testing the performance of the bio fuel cell.
Test2: Testing the performance of the CMOS chip.
Test3: Based on the results of Test 1 and 2, functional check that the bio fuel does not collapse after connecting CMOS chip.

By performing the above testing procedure, the supplier can guarantee the performance in advance and solve a known good die (KGD) issue.

III. Test-Chip Design and Measurement Setup

A. Test Chip Design

To verify the effectiveness of the proposed approach, a test chip was fabricated using 0.25-μm CMOS technology with a nominal supply voltage of 2.5 V. Fig. 10 shows a microphotograph of the test chip. The occupied footprints of

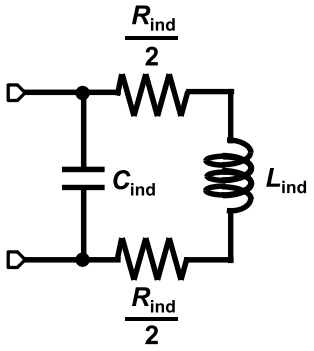

Fig. 9. Equivalent circuit model of the inductor used in this work.

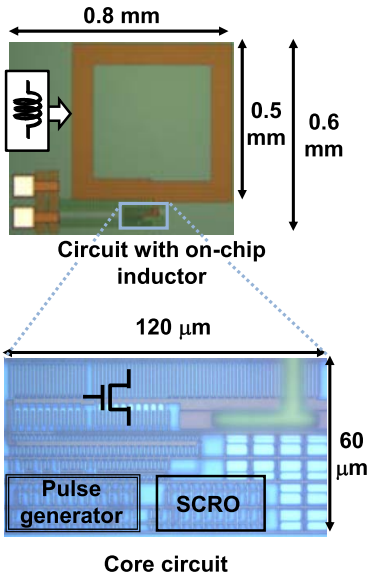

Fig. 10. Chip microphotograph of the proposed supply-sensing biosensor platform in 0.25 μm CMOS.

the core circuit without and with an on-chip inductor were 60 μm × 120 μm and 0.6 mm × 0.8 mm, respectively. In order to minimize the circuit footprint, we have not implemented any storage capacitors in this test chip. Although a storage capacitor will result in increase of circuit footprint, it will beneficial for more power consumption and longer communication distance. Thus, the designer can determine the implementation of a storage capacitor while taking this trade-off into account.

The test chip was assembled in a ceramic package. The diameter of the inductor is 0.5 mm and it has five turns. The calculated parameters in the equivalent circuit model (Fig. 9) is as follows: $L_{ind\_onchip} = 61$ nH, $R_{ind\_onchip} = 2.3\ \Omega$, $C_{ind\_onchip} = 810$ fF.

B. Measurement Setup

The measurement setup is shown in Fig. 11. Only two electrical signals, namely V_{DD} and V_{SS}, were supplied from the power supply (Key sight technologies, E3632A). To verify the transmitter operation using magnetic detection, a magnetic-field probe (Langer, H-Field probe MFA-K 0.1-12, 0.1-6 GHz) and a bias tee (Langer, Bias Tee) were employed.

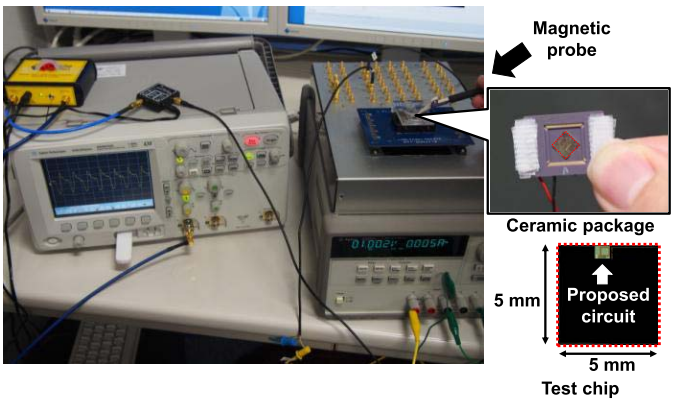

Fig. 11. Measurement setup. A magnetic probe was utilized to confirm the generation of magnetic flux from the test chip.

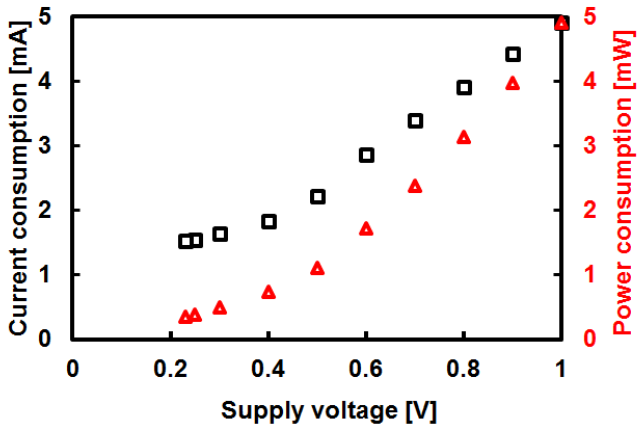

Fig. 12. Measured current and power consumption as a function of supply voltage. Operation at 0.23 V was verified.

The waveform was obtained using a sampling oscilloscope (Key sight technologies, DSO6102A). The measurement was performed under 20°C.

IV. Measurement Results

A. Results of the Functional Test

Fig. 12 shows the measured current and power consumption as a function of supply voltage. Operation with 0.23 V power supply was verified. A supply of 0.23 V is sufficiently low for self-powered operation using a bio fuel cell and is the lowest supply voltage ever reported for proximity communications. Because the drain current of a zero-V_{th} transistor is proportional to the square of gate-source voltage V_{GS} from 0 to 0.4 V and is proportional to V_{GS} from 0.4 V, the current consumption characteristics change at 0.4 V.

B. Performance Evaluation

The measured current consumed at 0.23 V was 1.52 mA, and the measured power is 0.35 mW, which can be obtained by a 1cm^2 of bio fuel cell [1], [2]. The measured average power consumption of the driver circuit is 0.33 mW. More than half is from leakage current. Fig. 13 shows the frequency of the output pulse from the magnetic field as a function of

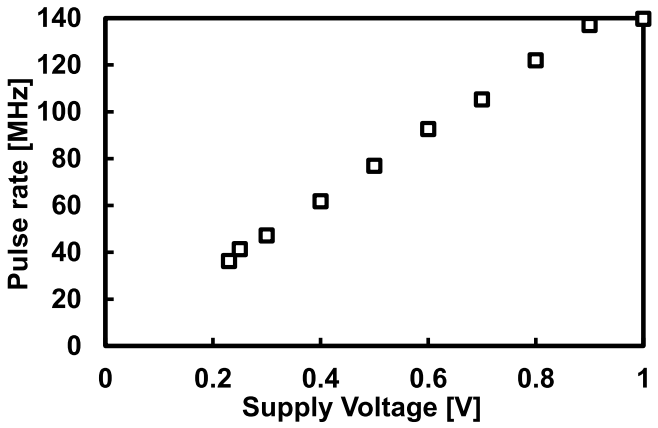

Fig. 13. Measured pulse-rate as a function of supply voltage.

TABLE I
SIMULATED RESULTS OF THE PERFORMANCE VARIATION DUE TO PROCESS, VOLTAGE, AND TEMPERATURE VARIATIONS

Process corner	FF	FS	TT	SF	SS
Minimum supply voltage [V] (27 °C)	0.20	0.26	0.22	0.29	0.30

Temperature	-40	27	125
Minimum supply voltage [V] (TT)	0.26	0.22	0.19

Process corner	FF	FS	TT	SF	SS
Pulse rate [MHz] (TT, 27 °C)	370	24	36	14	3.9

Temperature	-40	27	125
Pulse rate [MHz] (TT, 0.23 V)	1.0	36	840

supply voltage. The pulse rate decreases as supply voltage decreases with an almost linear relationship.

In order to investigate the performance variation, we have measured ten sample chips totally. Among ten sample chips, eight chips achieved 0.23-V operation while two chips achieved 0.22-V operation. Since we have utilized matured technology (0.25 μm CMOS technology), the performance variation was successfully mitigated.

The measurement results are obtained from the test chips that fabricated under normal (both NMOSs and PMOSs are typical, typical-typical, TT) condition. In order to investigate the performance variation due to process, voltage, and temperature, we have performed SPICE simulation.

Firstly, we have investigated minimum supply voltage under process and temperature variations. In TT condition, the simulated minimum supply voltage is 0.22 V. Under this condition, the simulated results are summarized in upper part of Table I. Secondly, the output pulse rate was investigated. The results are summarized in bottom part of Table I.

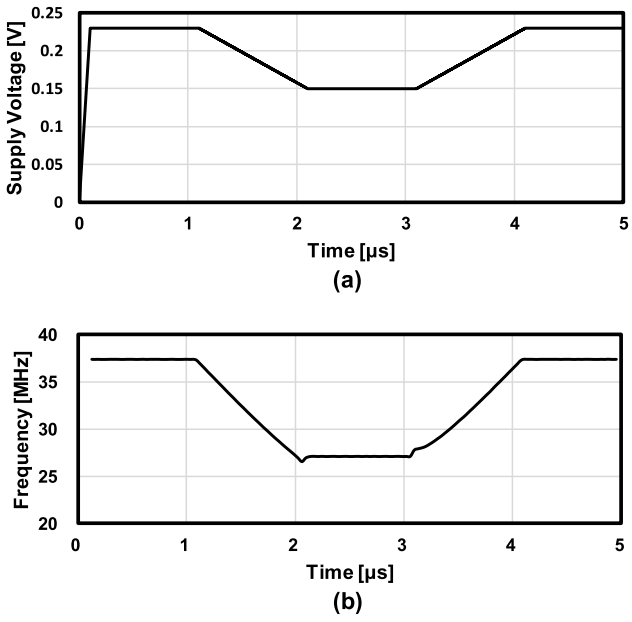

Fig. 14. Simulated performance of the cold-start capability. (a) Time trend of supply voltage (b) Oscillation frequency.

C. Discussion on Cold-Start

For evaluating performance of cold-starting, we have performed SPICE simulation. The simulation results are shown in Fig. 14. Fig. 14 (a) shows the time trend of supply voltage and Fig. 14 (b) shows the oscillation frequency. As shown in Fig. 14 (a), after the circuit started up when supply voltage is 0.23 V, we reduced the supply voltage to 0.15 V. Even when supply voltage becomes 0.15 V, the oscillation can continue. While, when the supply voltage becomes 0.14 V, the circuit does not function. The results indicate that the proposed circuit has functionality of cold start.

V. SELF-POWERED OPERATION USING BIO FUEL CELL

A. Performance of Organic Bio Fuel Cell

To verify the effectiveness of the proposed platform, self-powered operation using an organic bio fuel cell [1], [2] was demonstrated. The bio fuel cell has a cloth-like feature. The enzymes for energy generation were immobilized on the bio fuel cell. Fig. 14 shows a summary of the measured performance of the bio fuel cell. Figs. 14(a) and (b) are performance of the anode and cathode, respectively. Fig. 13(c) is the overall performance including both anode and cathode. By changing the load resistance, each measurement point was obtained. Fig. 14(d) shows the measurement setup. The measurement was performed using a three-electrode system (BSA, 730C electrochemical analyzer).

The bio fuel cell generates its energy from fructose. The sizes of the Anode and Cathodes of the bio fuel cell are 1-cm and 2-cm square, respectively. The sizes are optimized in order to function as a sensor, which is stated in Section II-B. The power peak is obtained at 0.3-0.4 V, which is a typical characteristic of bio fuel cells [1]–[3]. At the peak power condition, the power delivery capability of the bio fuel cell is approximately 0.33 mW.

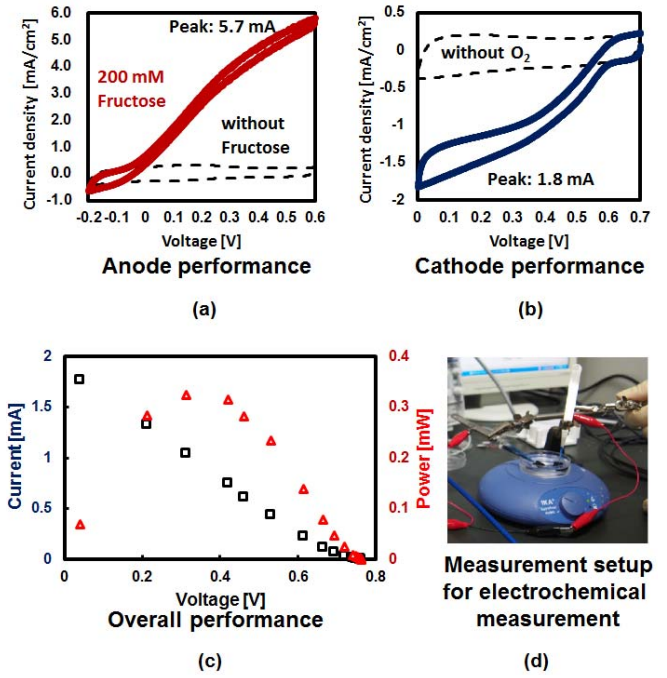

Fig. 15. Measured performance of the bio fuel cell and its measurement setup used to measure the results. (a) Anode performance (b) Cathode performance. (c) Overall performance (d) Measurement setup.

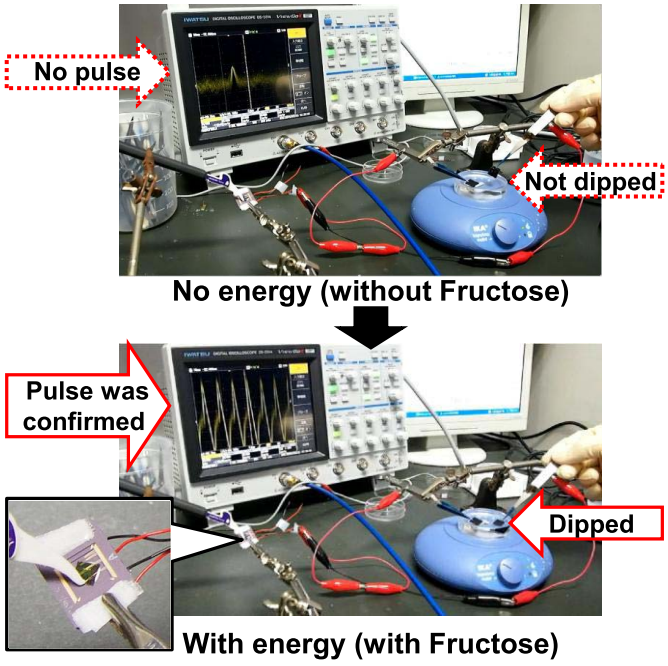

Fig. 16. Demonstration of self-powered operation using an organic bio fuel cell. When the bio fuel cell is dipped into a fructose solution, the proposed biosensor transmits a magnetic pulse.

The performance of the bio fuel cell can be modeled by a simple electrical circuit model as shown in Fig. 8(b). The extracted parameters are followings: $R_{\text{int}} = 380\Omega$ and $V_{\text{src}} = 0.78$ V.

B. Demonstration of Self-Powered Operation

Fig. 16 shows successful self-powered operation using the bio fuel cell. By dipping the bio fuel cell into a fructose solution, the circuit transmitted a magnetic field, and its waveform appeared on the oscilloscope. This work is the first demonstration of a self-powered CMOS-based proximity transmission using bio fuel cells and SCRO.

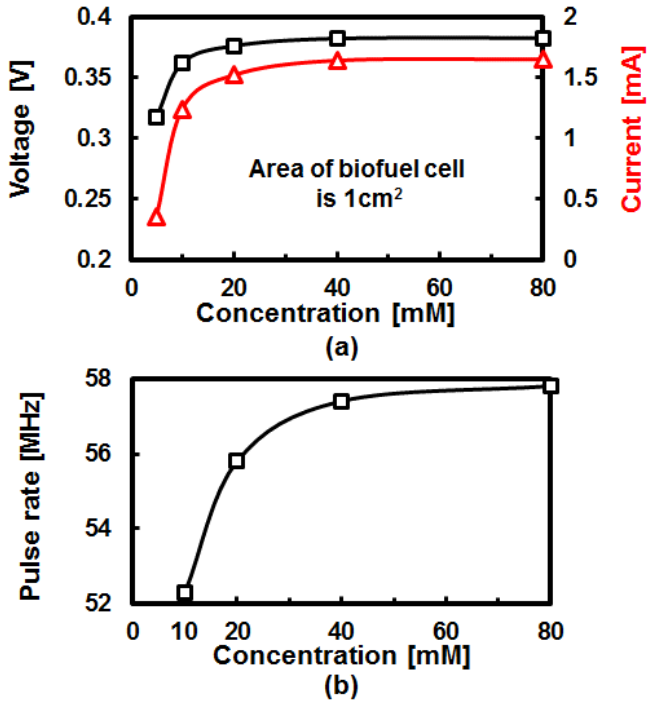

Fig. 17. Measured output voltage from bio fuel cell (a) and measured pulse rate (b) as a function of fructose concentration.

Fig. 17 shows a summary of the self-powered operation. Fig. 15(a) shows the output voltage and current of the bio fuel cell as a function of fructose concentration. The voltage and current increased as the fructose concentration increased. Fig. 15(b) shows the measured pulse rate of the output magnetic field from the proposed biosensor platform. The pulse rate increased as the fructose concentration increased. These results agree well with the performance of the platform shown in Fig. 12. From these measured results, we have successfully confirmed the feasibility of the proposed self-powered supply-sensing biosensor platform.

The leakage varies with respect of source voltage of the bio fuel cell. Since the monotonicity is guaranteed, this leakage variation does not affect the measurement of the specific variable as shown in the result in Fig. 17. For a more reliable reading, calibration must be performed.

We have confirmed that there is no issue with the circuit having an intermittent power, which was investigated by measurement. The cold start voltage is same as the minimum supply voltage. Even after having passed the cold start, the minimum supply voltage does not change.

VI. Design and Measurement Results of the Receiver

In order to verify the feasibility of the proposed supply-sensing biosensor platform, including its communication capability, we designed and fabricated another test chip using 0.25-μm CMOS technology.

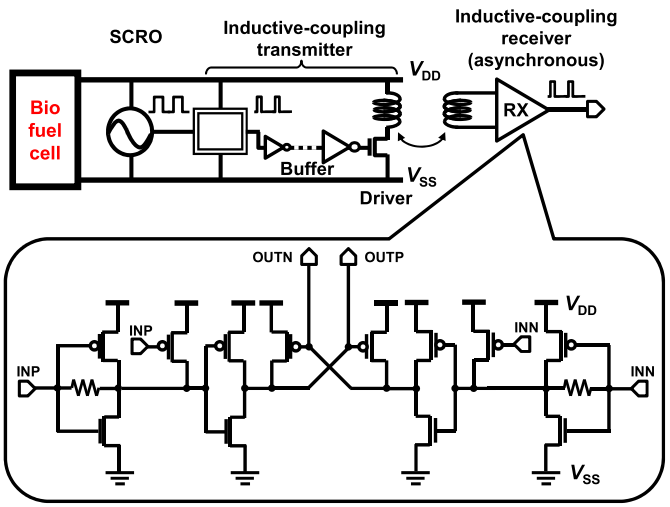

Fig. 18. Inter-chip communication between the proposed platform and asynchronous inductive-coupling receiver including the schematic of the implemented asynchronous inductive-coupling receiver.

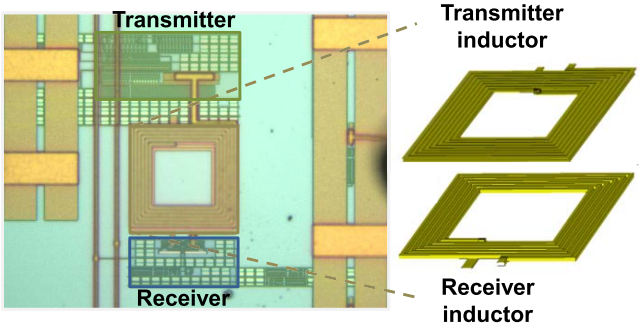

Fig. 19. Microphotograph of the test chip for verifying intra-chip communication between the proposed platform and asynchronous inductive-coupling receiver.

A. Design

As previously stated, the proposed supply-sensing biosensor platform adopts a time-domain signaling scheme and is not synchronous. Thus, the receiver must be asynchronous. Fig. 18 shows the schematic of the inter-chip communication system including the proposed supply-sensing biosensor platform and an inductive-coupling asynchronous receiver [18], which is based on a hysteresis comparator.

B. Test Chip Design and Measurement Setup

The test chip was fabricated using 0.25-μm CMOS technology. Fig. 19 shows the test chip microphotograph. The test chip contains the proposed biosensor platform and an intra-chip asynchronous inductive-coupling transceiver. The transmitter is 60 μm $\times$ 120 μm and the receiver is 45 μm $\times$ 100 μm. The inductor diameter is 100 μm. The communication distance between the transmitter and receiver inductor is approximately 5 μm. Since this transceiver is implemented in the same chip, the communication distance is limited to be short. However, if off-chip inductors are introduced, communication distance can be enlarged because communication distance of inductive-coupling transceiver is determined by the inductor size.

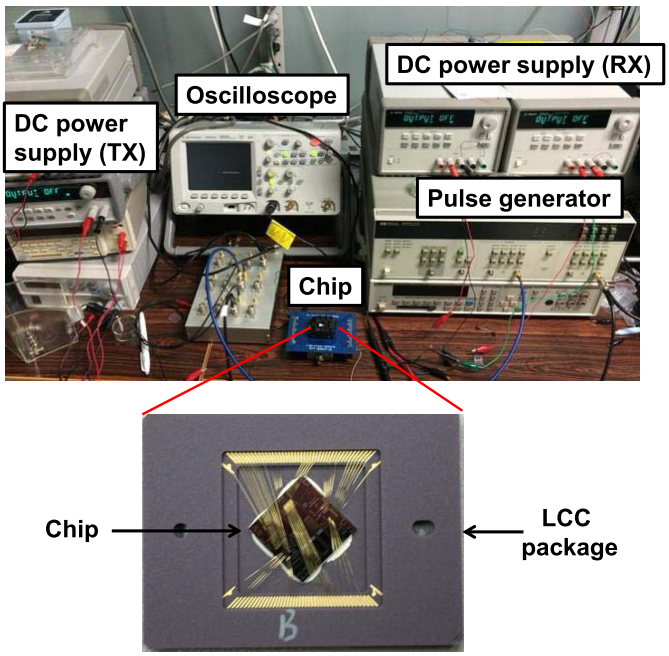

Fig. 20. Measurement setup for verifying intra-chip communication between the proposed platform and an asynchronous inductive-coupling receiver.

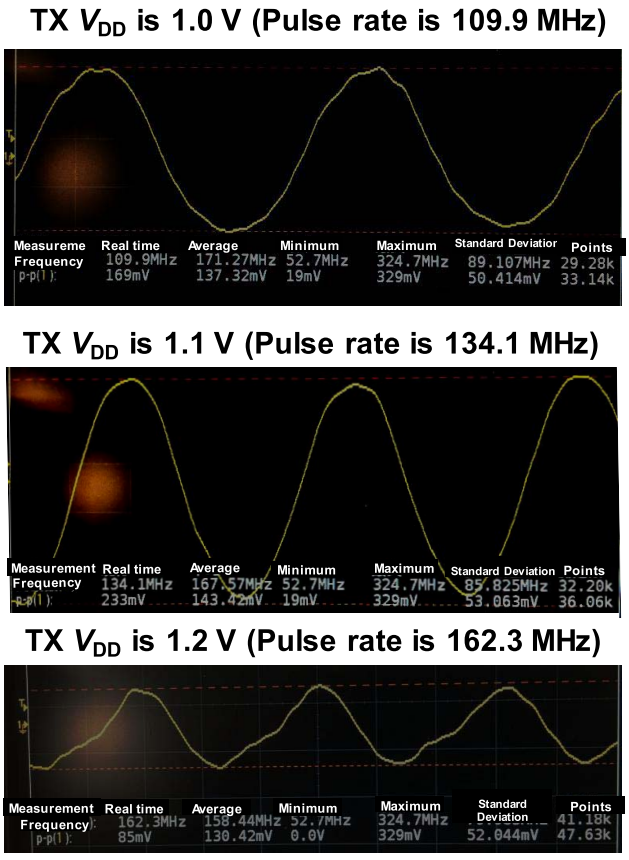

Fig. 21. Measured results of the received data of the intra-chip communication between the proposed platform and an asynchronous inductive-coupling receiver. The plots are from receiver side.

The measurement setup is shown in Fig. 20. The chip was packaged in a ceramic package, and the signal was fed into the chip from a pulse generator (Key sight technologies, 8131A).

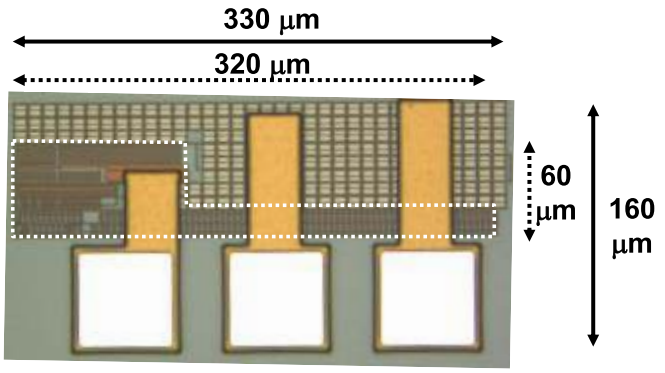

Fig. 22. Test chip microphotograph of the proposed platform without inductor.

The output signal from the chip was captured using a sampling oscilloscope (Key sight technologies, DSO6102A).

C. Measurement Results

Fig. 21 shows the measurement results of intra-chip communication, which shows that the receiver successfully detected the magnetic flux from the transmitter. The supply voltage of the receiver was 2.5 V, which is the nominal supply voltage of 0.25 μm CMOS technology. In our application, the receiver is expected to be implemented in a power-sufficient environment. Thus, the supply voltage of the receiver does not need to be low. In this measurement, the supply voltage of the proposed platform including the transmitter ranges from 1.0 V to 1.2 V.

As expected, the receiver can detect the change of the pulse rate as a function of the supply voltage of the proposed platform. The measurement results show that the communication system using the proposed platform is feasible.

VII. Design and Measurement Results of the Platform With an Off-Chip Inductor

To achieve further cost savings, we also designed and developed the proposed platform with an off-chip inductor.

A. Design

As stated above, an off-chip inductor is less expensive than an on-chip inductor because it does not occupy additional area on costly LSI chips. For instance, the on-chip inductor in the prototype as shown in Fig. 9 occupies almost 90% of the total area. Thus, by adopting an off-chip inductor, the occupied area can be reduced dramatically.

An off-chip inductor is designed in the same way as an on-chip inductor. First, the communication distance is determined by considering the target application. Next, the diameter is determined based on the communication distance. In general, the diameter should be larger than the communication distance. Third, the number of turns, line width and line space are determined. A SPICE simulation is then conducted using the equivalent circuit model (Fig. 8) of the inductor and its determined parameters.

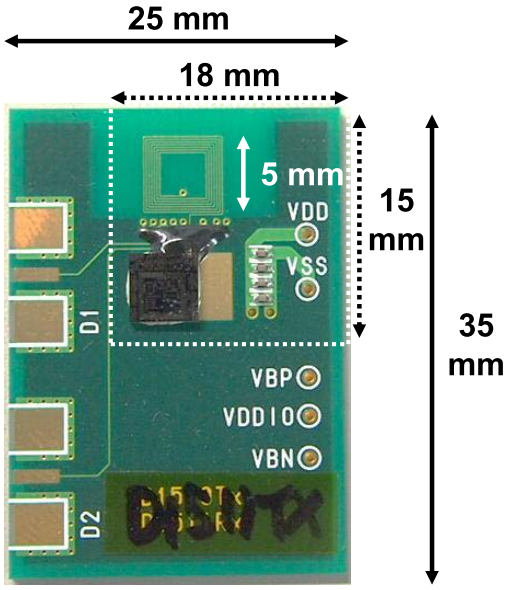

Fig. 23. Microphotograph of the proposed platform with an off-chip inductor on a PCB board.

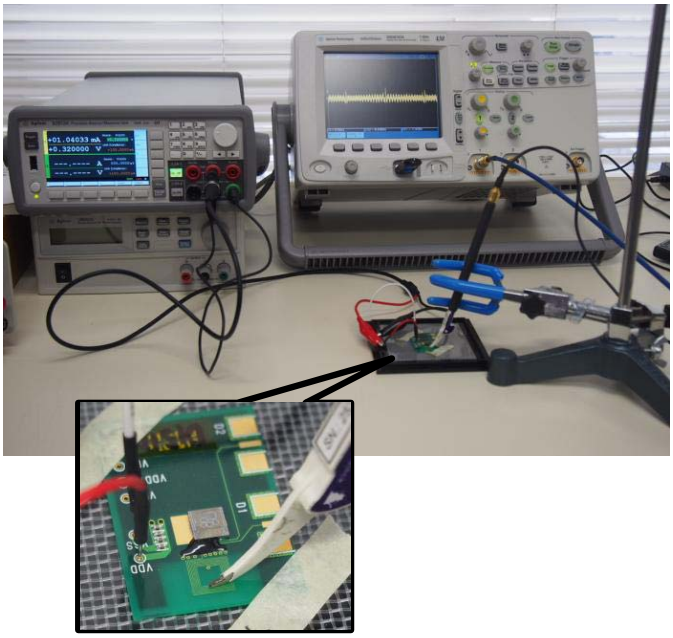

Fig. 24. Measurement setup for verifying the effectiveness of the proposed platform with an off-chip inductor.

B. Test Chip Design and Measurement Setup

The test chip was fabricated using 0.25-μm CMOS technology. Fig. 22 shows the test chip microphotograph. The test chip contains the proposed biosensor platform without an inductor. In order to reduce power consumption, there are 101 stages of the inverters in the SCRO. The transmitter core size is 60 μm $\times$ 320 μm and the total transmitter size including the I/O pads is 160 μm $\times$ 330 μm. The transmitter core is small enough to be easily implemented under the three I/O pads.

Fig. 23 shows the package of the prototype with an off-chip inductor. The chip was integrated onto the PCB board.

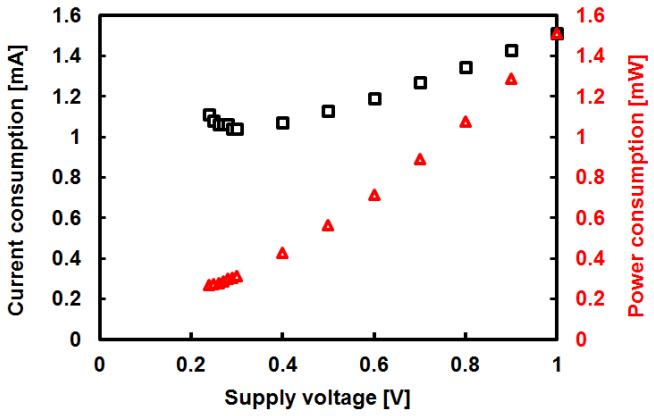

Fig. 25. Measured current and power consumption as a function of supply voltage of the proposed platform with an off-chip inductor. Operation at 0.24 V was verified.

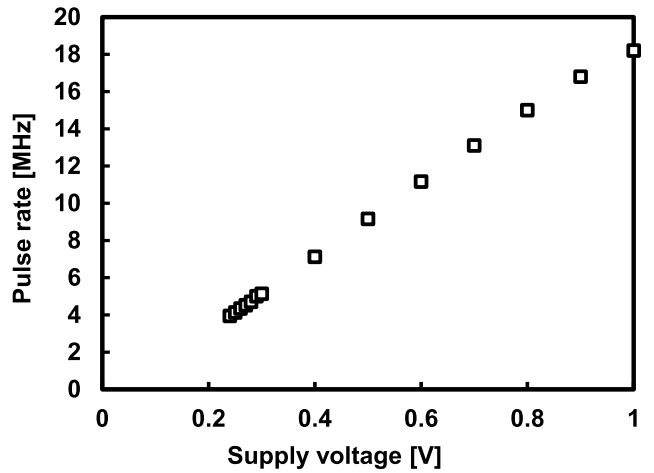

Fig. 26. Measured pulse rate as a function of supply voltage of the proposed platform with an off-chip inductor. Operation at 0.24 V was verified.

The inductor was fabricated using the interconnect of the PCB board. By adopting a PCB board with a thick metal (12 μm) interconnect, the resistance of the inductor can be reduced and low voltage operation can be achieved. The calculated parameters in the equivalent circuit model (Fig. 8) is as follows: $L_{\mathrm{ind_offchip}} = 380$ nH, $R_{\mathrm{ind_offchip}} = 1.8\ \Omega$, $C_{\mathrm{ind_offchip}} = 147$ fF.

The size of the entire PCB board is 35 mm$\times$ 25 mm, and the required size of the core PCB board without redundant part is 15 mm $\times$ 18 mm. The redundant parts are for compatibility with the integration of the receiver, which was not utilized in this work.

The measurement setup is shown in Fig. 24. A magnetic probe was utilized and placed over the interconnects of the off-chip inductor. The signal was fed into the chip from a pulse generator (Key sight technologies, 8131A). The output signal from the chip was captured using a sampling oscilloscope (Key sight technologies, DSO6102A).

C. Measurement Results

Fig. 25 shows the measurement results for the proposed platform with an off-chip inductor. Operation with 0.24-V power supply voltage was verified. Because the number of stages of the inverters in the SCRO is optimized for low power consumption in contrast to the prototype with on-chip inductor, the power consumption was lower than that of the prototype with an on-chip inductor.

Fig. 26 shows the measured pulse rate as a function of supply voltage. The almost linear relationship between the pulse rate and supply voltage was confirmed. The measurement results verify the feasibility of the proposed platform with an off-chip inductor, which would enable further cost reductions.

D. Discussion

When the off-chip inductors were utilized, the performance variation due to the angle of transmission is inevitable. About this issue, the literature [31] reported that the inductive-coupling link has high immunity on misalignment between the transmitter and receiver inductors. The performance variation due to the angle of transmission can be modeled as well as the misalignment since both result in degradation of the coupling coefficient. Thus, our proposed system may have sufficient immunity on the angle of transmission.

VIII. Conclusion

This paper demonstrated a self-powered, disposable, supply-sensing biosensor platform. The platform is based on a bio fuel cell and a zero-V_{th} all-digital CMOS SCRO with a current-driven, pulse-interval-modulated, inductive-coupling transmitter, that is able to operate under low-power supply voltage using legacy CMOS technology. Experiments using a 0.25-μm CMOS prototype chip demonstrated wireless transmission using a 0.23-V power supply, which is the lowest value for the power supply of a proximity transmitter ever reported. Self-powered operation using an organic bio fuel cell was also demonstrated. Additionally, the design and experimental verification of the receiver and off-chip inductor were experimentally verified.

Acknowledgment

The fabrication of CMOS chips was supported by Taiwan Semiconductor Manufacturing Co., Ltd. (TSMC, Taiwan), and the VLSI Design and Education Center (VDEC), University of Tokyo in collaboration with Synopsys, Inc. and Cadence Design Systems, Inc.

References

[1] X. Chen *et al.*, "A wireless capsule endoscope system with low-power controlling and processing ASIC," *IEEE Trans. Biomed. Circuits Syst.*, vol. 3, no. 1, pp. 11–22, Feb. 2009.

[2] S. B. Lee, H.-M. Lee, M. Kiani, U.-M. Jow, and M. Ghovanloo, "An inductively powered scalable 32-channel wireless neural recording system-on-a-chip for neuroscience applications," *IEEE Trans. Biomed. Circuits Syst.*, vol. 4, no. 6, pp. 360–371, Dec. 2010.

[3] A. Roy *et al.*, "A 6.45 μW self-powered SoC with integrated energy-harvesting power management and ULP asymmetric radios for portable biomedical systems," *IEEE Trans. Biomed. Circuits Syst.*, vol. 9, no. 6, pp. 862–874, Dec. 2015.

[4] Y. Ogawa *et al.*, "Organic transdermal iontophoresis patch with built-in biofuel cell," *Adv. Healthcare Mater.*, vol. 4, no. 4, pp. 506–510, Mar. 2015.

[5] T. Miyake, S. Yoshino, T. Yamada, K. Hata, and M. Nishizawa, "Self-regulating enzyme–nanotube ensemble films and their application as flexible electrodes for biofuel cells," *J. Amer. Chem. Soc.*, vol. 133, no. 13, pp. 5129–5134, Mar. 2011.
[6] T. Miyake *et al.*, "Enzymatic biofuel cells designed for direct power generation from biofluids in living organisms," *Energy Environ. Sci.*, vol. 4, no. 12, pp. 5008–5012, Dec. 2011.
[7] B. I. Rapoport, J. T. Kedzierski, and R. Sarpeshkar, "A glucose fuel cell for implantable brain–machine interfaces," *PLoS ONE*, vol. 7, no. 6, p. e38436, Jun. 2012.
[8] N. Miura, Y. Kohama, Y. Sugimori, H. Ishikuro, T. Sakurai, and T. Kuroda, "A high-speed inductive-coupling link with burst transmission," *IEEE J. Solid-State Circuits*, vol. 44, no. 3, pp. 947–955, Mar. 2009.
[9] Y.-T. Liao, H. Yao, A. Lingley, B. Parviz, and B. P. Otis, "A 3-μW CMOS glucose sensor for wireless contact-lens tear glucose monitoring," *IEEE J. Solid-State Circuits*, vol. 47, no. 1, pp. 335–344, Jan. 2012.
[10] H. Komori, K. Niitsu, J. Tanaka, Y. Ishige, M. Kamahori, and K. Nakazato, "An extended-gate CMOS sensor array with enzyme-immobilized microbeads for redox-potential glucose detection," in *Proc. IEEE Biomed. Circuits Syst. Conf.*, Oct. 2014, pp. 464–467.
[11] K. Niitsu, S. Ota, K. Gamo, H. Kondo, M. Hori, and K. Nakazato, "Development of microelectrode arrays using electroless plating for CMOS-based direct counting of bacterial and HeLa cells," *IEEE Trans. Biomed. Circuits Syst.*, vol. 9, no. 5, pp. 607–619, Oct. 2015.
[12] T. Tokuda *et al.*, "CMOS image sensor-based implantable glucose sensor using glucose-responsive fluorescent hydrogel," *Biomed. Opt. Exp.*, vol. 5, no. 11, pp. 3840–3870, Nov. 2014.
[13] F. Zhang and Y. Lian, "QRS detection based on multiscale mathematical morphology for wearable ECG devices in body area networks," *IEEE Trans. Biomed. Circuits Syst.*, vol. 3, no. 4, pp. 220–228, Aug. 2009.
[14] M. Khayatzadeh, X. Zhang, J. Tan, W.-S. Liew, and Y. Lian, "A 0.7-V 17.4-μW 3-lead wireless ECG SoC," *IEEE Trans. Biomed. Circuits Syst.*, vol. 7, no. 5, pp. 583–592, Oct. 2013.
[15] X. Zhang and Y. Lian, "A 300-mV 220-nW event-driven ADC with real-time QRS detection for wearable ECG sensors," *IEEE Trans. Biomed. Circuits Syst.*, vol. 8, no. 6, pp. 834–843, Dec. 2014.
[16] J. Tan, W.-S. Liew, C.-H. Heng, and Y. Lian, "A 2.4 GHz ULP reconfigurable asymmetric transceiver for single-chip wireless neural recording IC," *IEEE Trans. Biomed. Circuits Syst.*, vol. 8, no. 4, pp. 497–509, Aug. 2014.
[17] S. Izumi *et al.*, "Normally off ECG SoC with non-volatile MCU and noise tolerant heartbeat detector," *IEEE Trans. Biomed. Circuits Syst.*, vol. 9, no. 5, pp. 641–651, Oct. 2015.
[18] S. Izumi *et al.*, "A wearable healthcare system with a 13.7 μA noise tolerant ECG processor," *IEEE Trans. Biomed. Circuits Syst.*, vol. 9, no. 5, pp. 733–742, Oct. 2015.
[19] K. Niitsu, A. Kobayashi, Y. Ogawa, M. Nishizawa, and K. Nakazato, "An energy-autonomous, disposable, big-data-based supply-sensing biosensor using bio fuel cell and 0.23-V 0.25-μm zero-V_{th} all-digital CMOS supply-controlled ring oscillator with inductive transmitter," in *IEEE Biomed. Circuits Syst. Conf. (ISSCC) Dig. Tech. Papers*, Oct. 2015, pp. 595–598.
[20] N. Miura, D. Mizoguchi, M. Inoue, H. Tsuji, T. Sakurai, and T. Kuroda, "A 195Gb/s 1.2W 3D-stacked inductive inter-chip wireless superconnect with transmit power control scheme," in *IEEE Int. Solid-State Circuits Conf. (ISSCC) Dig. Tech. Papers*, Feb. 2005, pp. 264–265.
[21] A. Iwata *et al.*, "A 3D integration scheme utilizing wireless interconnections for implementing hyper brains," in *IEEE Int. Solid-State Circuits Conf. (ISSCC) Dig. Tech. Papers*, Feb. 2005, pp. 262–263.
[22] N. Miura *et al.*, "A 1 Tb/s 3 W inductive-coupling transceiver for 3D-stacked inter-chip clock and data link," *IEEE J. Solid-State Circuits*, vol. 42, no. 1, pp. 111–122, Jan. 2007.
[23] K. Niitsu *et al.*, "60% power reduction in inductive-coupling inter-chip link by current-sensing technique," *Jpn. J. Appl. Phys.*, vol. 46, no. 4B, pp. 2215–2219, Apr. 2007.
[24] K. Niitsu *et al.*, "Daisy chain transmitter for power reduction in inductive-coupling CMOS link," *IEICE Trans. Electron.*, vol. E90-C, no. 4, pp. 829–835, Apr. 2007.
[25] D. Hopkins *et al.*, "Circuit techniques to enable 430 Gb/s/mm^2 proximity communication," in *IEEE Int. Solid-State Circuits Conf. (ISSCC) Dig. Tech. Papers*, Feb. 2007, pp. 368–369.
[26] A. Fazzi *et al.*, "3D capacitive interconnections with mono- and bi-directional capabilities," in *IEEE Int. Solid-State Circuits Conf. (ISSCC) Dig. Tech. Papers*, Feb. 2007, pp. 356–357.
[27] Q. Gu, Z. Xu, J. Ko, and M.-C. F. Chang, "Two 10Gb/s/pin low-power interconnect methods for 3D ICs," in *IEEE Int. Solid-State Circuits Conf. (ISSCC) Dig. Tech. Papers*, Feb. 2007, pp. 448–449.
[28] M. Daito *et al.*, "Capacitively coupled non-contact probing circuits for membrane-based wafer-level simultaneous testing," in *IEEE Int. Solid-State Circuits Conf. (ISSCC) Dig. Tech. Papers*, Feb. 2010, pp. 144–145.
[29] K. Niitsu, S. Kawai, N. Miura, H. Ishikuro, and T. Kuroda, "A 65fJ/b inter-chip inductive-coupling data transceivers using charge-recycling technique for low-power inter-chip communication in 3-D system integration," *IEEE Trans. Very Large Scale Integr. (VLSI) Syst.*, vol. 20, no. 7, pp. 1285–1294, Jul. 2012.
[30] K. Niitsu *et al.*, "An inductive-coupling link for 3D integration of a 90 nm CMOS processor and a 65 nm CMOS SRAM," in *IEEE Int. Solid-State Circuits Conf. (ISSCC) Dig. Tech. Papers*, Feb. 2009, pp. 480–481.
[31] K. Niitsu *et al.*, "Modeling and experimental verification of misalignment tolerance in inductive-coupling inter-chip link for low-power 3-D system integration," *IEEE Trans. Very Large Scale Integr. (VLSI) Syst.*, vol. 18, no. 8, pp. 1238–1243, Aug. 2010.
[32] K. Niitsu *et al.*, "Analysis and techniques for mitigating interference from power/signal lines and to SRAM circuits in CMOS inductive-coupling link for low-power 3-D system integration," *IEEE Trans. Very Large Scale Integr. (VLSI) Syst.*, vol. 19, no. 10, pp. 1902–1907, Oct. 2011.
[33] M. Saen *et al.*, "3-D system integration of processor and multi-stacked SRAMs using inductive-coupling link," *IEEE J. Solid-State Circuits*, vol. 45, no. 4, pp. 856–862, Apr. 2010.
[34] Y. Kohama *et al.*, "A scalable 3D processor by homogeneous chip stacking with inductive-coupling link," in *Proc. IEEE Symp. VLSI Circuits*, Jun. 2009, pp. 94–95.
[35] N. Miura *et al.*, "A 0.55 V 10 fJ/bit inductive-coupling data link and 0.7 V 135 fJ/cycle clock link with dual-coil transmission scheme," *IEEE J. Solid-State Circuits*, vol. 46, no. 4, pp. 965–973, Apr. 2011.
[36] T. A. Wey, M. Southcott, W. D. Jemison, K. MacVittie, and E. Katz, "Electrical circuit model and dynamic analysis of implantable enzymatic biofuel cells operating *in vivo*," *Proc. IEEE*, vol. 102, no. 11, pp. 1795–1810, Nov. 2014.

Kiichi Niitsu (S'05–M'10) was born in Japan, in 1983. He received the B.S. degree *(summa cum laude)*, M.S. and Ph.D. degrees in electrical engineering from Keio University, Yokohama, Japan, in 2006, 2008, and 2010, respectively. From 2008 to 2010, he was a Research Fellow with the Japan Society for the Promotion of Science, a Research Assistant of the Global Center of Excellence Program, Keio University, and a Collaboration Researcher with the Keio Advanced Research Center. From 2010, he was an Assistant Professor with Gunma University, Kiryu, Japan. Since 2012, he has been a Lecturer with Nagoya University, Nagoya, Japan. Since 2015, he has been a Researcher with Precursory Research for Embryonic Science and Technology, Japan Science and Technology Agency. His current research interest lies in the low-power and high-speed technologies of analog and digital VLSI circuits for biomedical application.

He was a recipient of the 2006 KEIO KOUGAKUKAI Award, the 2007 INOSE Science Promotion Award, the 2008 IEEE SSCS Japan Chapter Young Researcher Award and the 2009 IEEE SSCS Japan Chapter Academic Research Award from IEEE Solid-State Circuits Society Japan Chapter, the 2008 FUJIWARA Award from the FUJIWARA foundation, the 2011 YASUJIRO NIWA Outstanding Paper Award, the 2011 FUNAI Research Promotion Award, the 2011 Ando Incentive Prize for the Study of Electronics, the 2011 Ericsson Young Scientist Award, the 2012 ASP-DAC University LSI Design Contest Design Award, the NF Foundation Research and Development Encouragement Award, the AKASAKI Award from Nagoya University, the IEEE Nagoya Section Young Researcher Award, the IEEE Biomedical Circuits and Systems Conference 2016 (BioCAS 2016) Best Paper Award, the 2017 Commendation for Science and Technology by the Minister of Education, Culture, Sports, Science and Technology, the Young Scientists Prize, the 2018 SUEMATSU-Yasuharu Award from IEICE.

He has authored or co-authored 51 referred original journal papers, 111 international conference papers, and three book chapters, including two TBioCAS, one TCAS-I, five JSSC, five TVLSI, two ISSCC, four Symp. On VLSI Circuits, nine BioCAS, one ISCAS, and four A-SSCC. He served as a technical committee of the IEEE biomedical circuits and systems (BioCAS TC), a Review Committee Member of ISCAS 2017/2018, a Technical Program Committee of ICECS 2018, a Review Committee Member of APCCAS 2014, an editorial committee of IEICE Transactions on Electronics, Special Section on Analog Circuits and Related SoC Integration Technologies, and an editorial committee of IEICE ESS Fundamental Review. He is a member of the Institute of Electronics, Information and Communication Engineers of Japan and the Japan Society of Applied Physics.

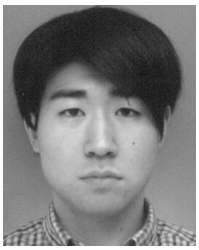

Atsuki Kobayashi (S'16) was born in Yamanashi, Japan, in 1993. He received the B.S. degree in electrical engineering and computer science from Nagoya University, Nagoya, Japan, in 2016, where he is currently pursuing the M.S. degree. His research activity is focused on mixed-signal CMOS integrated circuits for biomedical applications.

Yuya Nishio (S'18) was born in Japan in 1996. He is currently pursuing the B.S. degree in electrical engineering and computer science from Nagoya University, Nagoya, Japan. His research activity is focused on mixed-signal CMOS integrated circuits for biomedical applications.

Kenya Hayashi (S'18) was born in Japan in 1995. He is currently pursuing the B.S. degree in electrical engineering and computer science from Nagoya University, Nagoya, Japan. His research activity is focused on mixed-signal CMOS integrated circuits for biomedical applications.

Kei Ikeda (S'16) was born in Japan in 1992. He received the B.S. degree in electrical engineering and computer science from Nagoya University, Nagoya, Japan, in 2016, where he is currently pursuing the M.S. degree. His research activity is focused on mixed-signal CMOS integrated circuits for biomedical applications.

Takashi Ando was born in Japan. He received the B.S. degree in electrical engineering and computer science from Nagoya University, Nagoya, Japan, in 2015, where he is currently pursuing the M.S. degree. His research activity is focused on mixed-signal CMOS integrated circuits for biomedical applications.

Yudai Ogawa was born in Japan in 1988. He received the B.S. degree from Kumamoto University, Kumamoto, Japan, in 2011, and the M.S. and Ph.D. degrees from Tohoku University, Sendai, Japan, in 2013 and 2016, respectively, all in mechanical engineering. His current research interests include biofuel cells, enzyme electrodes, flexible electronics, stretchable electronics, carbon nanomaterials, and cell engineering.

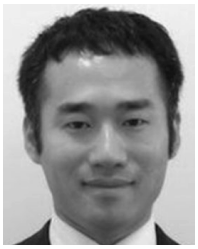

Hiroyuki Kai was born in Japan in 1984. He received the B.Eng. and M.Eng. degrees in chemistry and biotechnology from The University of Tokyo, in 2006 and 2008, respectively, and the Ph.D. degree in chemistry from the University of California at Berkeley, Berkeley, CA, USA, in 2015. His research interests include soft, wearable electronics and sensors based on organic and materials chemistry.

Matsuhiko Nishizawa was born in 1965. He received the B.S., M.S., and Ph.D. degrees in applied chemistry from Tohoku University, Japan. From 1995, he was a Research Assistant with Osaka University, and moved to Tohoku University in 1997. Since 2003, he has been a Professor with the Department of Biorobotics, Tohoku University. His main concern is BioMEMS technology, including the biological batteries and biocompatible hydrogel electrodes, and its application in medical and healthcare fields. He received the 2000 Young Researcher Award from the Chemical Society of Japan, the 2000 Young Researcher Award from the Electrochemical Society of Japan, and the 2016 Academic Award from the Chemical Society of Japan.

Kazuo Nakazato was born in Japan in 1952. He received the B.S., M.S., and Ph.D. degrees in physics from the University of Tokyo, in 1975, 1977, and 1980, respectively. In 1981, he joined the Central Research Laboratory, Hitachi Ltd., Tokyo, involved in high-speed silicon self-aligned bipolar devices SICOS (sidewall base contact structure), which were adopted in main frame computer Hitachi M-880/420. In 1989, he moved to the Hitachi Cambridge Laboratory, Hitachi Europe Ltd., Cambridge, U.K., as a Senior Researcher and the Laboratory Manager, involved in experimental and theoretical study of quantum electron transport in semiconductor nano structures, including single-electron memory. Since 2004, he has been a Professor of intelligent device with the Department of Electrical Engineering and Computer Science, Graduate School of Engineering, Nagoya University, Japan. His main concerns are BioCMOS technology, single molecule-CMOS hybrid devices, and CMOS analog circuits for integrated sensors.